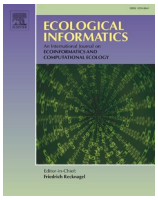
Ecological Informatics 84 (2024) 102867



Contents lists available at ScienceDirect

Ecological Informatics

journal homepage: www.elsevier.com/locate/ecolinf



A multi-source approach to mapping habitat diversity: Combination of multi-date multispectral satellite imagery and comparison with single-date hyperspectral results in a Mediterranean Natural Reserve

Chiara Zabeo [a,*], Gaia Vaglio Laurin [a,b], Birhane Gebrehiwot Tesfamariam [a], Diego Giuliarelli [a], Riccardo Valentini [a], Anna Barbati [a]

[a] Department for Innovation in Biological, Agro-food, and Forestry Systems, Tuscia University, Via San Camillo De Lellis snc, 01100 Viterbo, VT, Italy
[b] Research Institute on Terrestrial Ecosystems, National Research Council, Montelibretti Research Area, Via Salaria Km 29,300, 00015 Montelibretti, RM, Italy

ARTICLE INFO

Keywords:
Habitat mapping
Hyperspectral
Vegetation spectroscopy
Spaceborne
Multispectral
Spectral indices

ABSTRACT

The increasing availability of spaceborne hyperspectral satellite imagery opens new opportunities for forest habitat mapping and monitoring, but the limitation of its generally low temporal resolution must be considered. In this study, we compare the ability of single-date PRISMA (PRecursore IperSpettrale della Missione Applicativa), the hyperspectral satellite from the Italian Space Agency, with that of both single-date and multi-date Sentinel-2 (S2) and PlanetScope (PS) to detect and correctly classify various EUNIS habitat types distributed over a relatively small spatial extent (6000 ha) in a natural reserve in Central Italy. The case study deals with multiple levels of spectral similarity, as the dominant canopy species of the target forest habitat classes belong to the same genus (*Quercus* spp., both deciduous and evergreen species) as well as of different taxa (*Pinus* and *Fraxinus* spp.). We performed a pixel-based classification with the Random Forest algorithm using a set of 22 spectral indices computed on S2, and 12 on PS, and compared the results with those obtained by PRISMA (28 indices). A Canopy Height Model (CHM) was also used as an input variable for the classification. The single date classification of PlanetScope obtained lower overall accuracy (69 %) than what obtained with other sensors (PRISMA and Sentinel-2) in a previous study over the same area. Regarding the comparison between multi-date multispectral and single-date hyperspectral, 10-fold cross-validation results revealed that S2 achieves an out-of-bag error rate of approximately 16 %, and PS 19 %, while PRISMA result from previous study achieves 17 %. This demonstrates that a combination of spectral indices calculated during the growing season can capture phenological or physiological differences among the target species, which consequently results in a significant improvement in the classification accuracy of the multispectral sensors. Ultimately, classification results from all three sensors were combined to create probability maps for each forest class, identifying areas classified with a higher degree of certainty by each satellite tested and potentially contributing to forest management by defining areas with varying conservation levels.

1. Introduction

Canopy plants are the dominant primary producers in forest ecosystems and provide habitat for a variety of other taxa. The floristic composition of plant communities is regarded as a proxy for vegetated ecosystem diversity (European Environmental Agency (EEA), 2014) and is widely used as a diagnostic key for the classification and mapping of natural and semi-natural terrestrial habitats in Europe, within Annex 1 of the EU Habitat Directive (92/43/EEC) or EUNIS habitat classifications (Chytrý et al., 2020).

Based on the assumption that spectral heterogeneity closely correlates with biodiversity (Warren et al., 2014), remote sensing offers a clear advantage for monitoring forest habitat extent, provided that relationships between habitat characteristics and spectral properties are established. Following the "spectral species" concept (Rocchini et al., 2021), the discrimination of compositional differences in forest canopy from optical imagery is primarily determined by the similarity or uniqueness of the biochemical composition and structural properties of

* Corresponding author.
E-mail address: chiara.zabeo@unitus.it (C. Zabeo).

https://doi.org/10.1016/j.ecoinf.2024.102867
Received 17 July 2024; Received in revised form 22 October 2024; Accepted 22 October 2024
Available online 24 October 2024
1574-9541/© 2024 The Author(s). Published by Elsevier B.V. This is an open access article under the CC BY license (http://creativecommons.org/licenses/by/4.0/).

the foliage among tree species (Asner and Martin, 2016; Somers and Asner, 2014). This has been demonstrated by a recent study (Schweiger and Laliberté, 2022), which revealed that spatial variation in plot-level reflectance captures changes in plant species composition at the scale of currently operational satellite missions (30 × 30 m pixels), such as PRISMA or ENMAP, and that this relationship holds across biomes, including ecosystems dominated by forests, shrubs, and grassland. Furthermore, D'odorico et al. (2023) found that leaves at the top of the canopy have superior discrimination capacity compared to bottom-of-canopy leaves. This holds potential for distinguishing species-specific traits through spaceborne remote sensing, despite the drawback of background signals and acquisition geometry, which may complicate the classification task.

Operational hyperspectral imaging satellite missions (PRISMA, ENMAP) open new avenues for analysing top-of-canopy tree composition, thanks to the ability of hyperspectral data to measure the spectral reflectance of plant canopies over hundreds of bands from the visible to the near-infrared and shortwave-infrared regions of the electromagnetic spectrum. The PRISMA sensor (PRecursore IperSpettrale della Missione Applicativa), launched in March 2019 by the Italian Space Agency (ASI), is a medium-resolution (30 m) hyperspectral imaging satellite with over 200 bands operating in the VNIR/SWIR, with a bandwidth of around 12 nm (ASI, 2020; Cogliati et al., 2021; Coppo et al., 2019). This seamless "keyboard" of narrow spectral bands can help detect very specific chemical signals and compounds, which are usually not captured by broad-band multispectral satellites. PRISMA imagery has been used for applications in the fields of geology (Tripathi and Garg, 2021), ecology (Arasumani et al., 2023), water quality monitoring (Amieva et al., 2023; Begliomini et al., 2023; de Lima et al., 2023), agriculture (Pepe et al., 2020), and environmental sciences (de Abreu Araújo et al., 2023; Hovi et al., 2023; Lazzeri et al., 2021; Quintano et al., 2023; Vangi et al., 2021), while its application to forest canopy composition mapping is still emerging (e.g., Vaglio Laurin et al., 2024).

However, the moderate spatial resolution of the hyperspectral sensor is a limitation for detecting habitat types with fragmented spatial patterns. Furthermore, as image pixels can be thought of as a mix of tree crowns from more than one individual, the sensor's ability to detect compositional differences in the forest canopy is expected to depend on the spectral similarity of the species to be separated, which is significantly associated with the phylogenetic similarity among species (Cavender-Bares et al., 2016). Lastly, the PRISMA mission currently operates with on-demand tasking acquisitions within quota limits. Only a limited number of products are available for each project, thus excluding the possibility of collecting a regular time series and raising the need to contemplate the use of additional optical data sources with a regular acquisition pattern.

Taking all these factors into account, it seems crucial to explore whether the narrower spectral bands of a single-date PRISMA acquisition perform better in forest habitat mapping than multiple acquisitions of multispectral images. Our overarching goal is to assess whether forest habitats dominated by single species or tree assemblages from a variety of plant taxa can be satisfactorily mapped by a single-date acquisition of PRISMA or by seasonal time-series acquired from Sentinel-2 (S2) and the commercial PlanetScope (PS) constellations. These two multispectral Earth observations (EO) satellites, unlike PRISMA, have regular acquisition patterns, acquiring imagery respectively every 2 to 5 days and daily. The comparison of PRISMA with S2 and PS is justified by the hypothesis that time series can capture seasonal dynamics of canopy reflectance properties that may be relevant for the discrimination of compositional differences in the forest canopy, as demonstrated in earlier studies (Haddad et al., 2022; Rapinel et al., 2019).

Several studies have explored habitat mapping with S2, either on its own (Arasumani et al., 2024; Bartold and Kluczek, 2024; Bayle et al., 2019; Le Dez et al., 2021; Marcinkowska-Ochtyra et al., 2023; Marian et al., 2024; Marzialetti et al., 2019; Pesaresi et al., 2022; Pesaresi et al., 2024; Rapinel et al., 2019; Tran et al., 2024; Xia and Lv, 2024) or in combination with, or comparison to, other platforms (Aditya et al., 2021; Ahmed et al., 2022; Arasumani et al., 2023; Iglseder et al., 2023; Jarocińska et al., 2023; Kycko et al., 2022; Prodromou et al., 2024; Punalekar et al., 2024; Torresani et al., 2019). Sentinel-2, a mission by the European Space Agency (ESA) ongoing since late 2015, offers open-source data with a relatively high temporal resolution (2 to 5 days). Its Multispectral Instrument (MSI), which includes 13 bands covering the visible to the short-wave infrared (SWIR) spectrum, and its generally medium spatial resolution (four bands at 10 m, six at 20 m, and three at 60 m), has proven suitable for mapping different types of habitats worldwide, using either the original spectral bands or vegetation indices (VIs). However, in most studies using VIs, only NDVI or a few of the many indices computable with S2 bands are employed in the classification procedure, and the number of classes considered is often limited.

In recent years, habitat mapping has also been carried out with PS (Doughty et al., 2024; Haddad et al., 2022; Szostak et al., 2021). The PlanetScope mission consists of a constellation of small satellites called Doves (4-band) or SuperDoves (8-band), covering the visible and near-infrared (NIR) regions, which acquire daily high-resolution (3 m) images on a global scale. Currently, the number of studies utilizing this sensor is limited due to the commercial nature of the mission (although a monthly quota of data is available for research and educational purposes). In these cases too, broad categories and few VIs were considered.

Only Vaglio Laurin et al. (2024) demonstrated that PRISMA outperforms S2 in single-capture mapping of diverse forest habitat types, leveraging spectral indices and a Canopy Height Model (CHM) within a Random Forest (RF) classification framework, in the same study area. Replicating the single date classification carried out with PRISMA and S2 in the same study area, which exhibits a complex spatial pattern of forest and other natural habitats, this study delves deeper into the comparison of PRISMA, S2, and PS imagery. Based on previous studies involving hyperspectral imagery (Aditya et al., 2021; Arasumani et al., 2023; Jarocińska et al., 2023; Vangi et al., 2021), PRISMA is expected to outperform the multispectral sensors. However, since the multitemporal aspect of the latter has not been considered in previous comparison studies, this warrants further clarification.

Previous studies have investigated the trade-offs between different sensor characteristics and compared their performance in habitat and species-specific mapping (Meerdink et al., 2024; Torresani et al., 2019; Vanguri et al., 2024). However, to our knowledge, this is the first study that comprises an all-round comparison of three sensors' characteristics, including their spectral, spatial, and temporal aspects, and includes recently launched satellites such as those investigated here. The specific goals of this study are to:

i) Compare the performance of two EO satellites for forest habitat mapping using the Random Forest classification to identify the trade-offs between the spectral, spatial, and temporal resolutions offered by each satellite: S2 (medium spatial/temporal, 13 bands VIS-SWIR), and PS (high spatial/temporal, 8 bands VIS-NIR). Results are also compared with those obtained over the same area by a previous study using S2 and PRISMA hyperspectral single-dates;
ii) Compare the two multispectral satellites, focusing on how the increased number of spectral bands in S2, particularly those in the short-wave infrared (SWIR) region, may improve classification accuracy compared to PS;
iii) Evaluate how the availability of a time series from the two multispectral sensors influences classification accuracy compared to the single-date imagery of PRISMA;
iv) Identify which indices, and thus which regions of the electromagnetic spectrum, contribute most to classification accuracy, and how they differ among the three sensors.

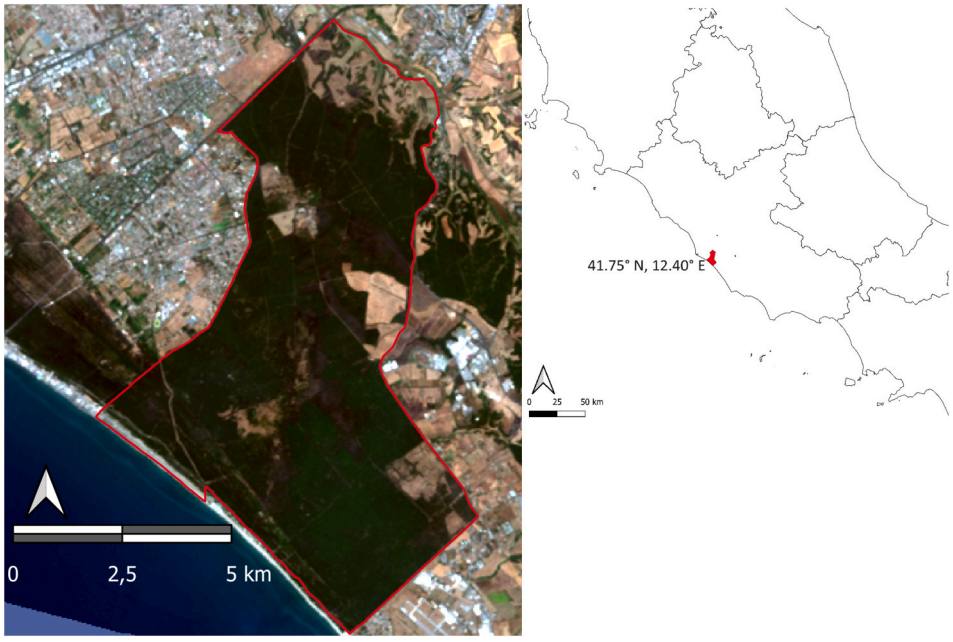


Fig. 1. Location and boundaries of the Castelporziano Natural Reserve. True colour PRISMA composite from 14/07/2022 (R: B32, G: B18, B: B8).

2. Material and methods

2.1. Study area

The study area is the Castelporziano Natural Reserve, located southwest of the Metropolitan City of Rome (Fig. 1), covering more than 6000 ha. It contains a variety of Mediterranean forest habitats, as well as two sites of community importance (SCIs): the coastal area and the lowland oak forest. Due to its history, first as a Papal estate and then as a hunting reserve for the Italian Royal family until its declaration as a Natural Reserve in 1999, the area has remained substantially unchanged over the years and preserves within its borders what remains of the forest system that once characterized the Tiber River delta and neighbouring zones (Recanatesi et al., 2020), thereby representing a unique opportunity to study and monitor these habitats.

A large portion of the area (more than 2000 ha, Scrinzi et al., 2019) is covered by the aforementioned deciduous oak forest, composed mainly of *Quercus robur* L. and *Quercus frainetto* Ten., with other accompanying broadleaf species such as *Carpinus betulus* L. and *Fraxinus* spp. This habitat in coastal Italy represents a relic of ancient plain forests that used to exist in the area (Recanatesi et al., 2020). Another considerable portion is covered by *Pinus pinea* L. stands, which have been declining since 2017 due to attacks by *Tomicus destruens* Woll. (Recanatesi et al., 2019). Evergreen oak forests are present as distinct *Quercus ilex* L. and *Quercus suber* L. stands, as well as Mediterranean maquis near the coast. Agroforestry practices have been implemented in the past (Gratani et al., 2017; Pignatti et al., 2015), which has led to the presence of *Eucalyptus* spp. and *Q. suber* plantations, as well as pastures for local cattle.

This study adopted the EUNIS habitat nomenclature (Level 3, 2021 revision) from the European Environment Agency's (EEA) European Nature Information System (EUNIS) for forest and natural habitat classification (https://eunis.eea.europa.eu/habitats.jsp). Replicating the approach used by Vaglio Laurin et al. (2024), the EUNIS habitat map was obtained by assigning a EUNIS 2021 code to classes in the Castelporziano Forest Management Plan (FMP) map, which depicts the spatial distribution of the main vegetation types (forest, shrubland, grassland) and other land uses in the Castelporziano Presidential Estate. The FMP map, provided by the Presidential Estate Scientific Committee and considered the reference ground truth, depicts vegetation types and land uses in the estate using field sampling, dominant canopy species, and very high-resolution aerial photograph interpretation (Giordano et al., 2010; Scrinzi et al., 2016, 2019). The map was updated to reflect pine habitat changes due to sanitation cuts. The two deciduous oak classes from Vaglio Laurin et al. (2024), which are spectrally and structurally similar, were merged into T195 based on their findings. The revised reference ground truth map for this study comprised 17 classes in total, of which 7 were forest habitats and 10 were other land cover types (Table 1).

Considering the results of Vaglio Laurin et al. (2024), the Random Forest (RF, Breiman, 2001) algorithm was chosen as the machine learning method. Among the advantages of RF is its ability to avoid overfitting, minimize the time required to classify satellite images, and produce reliable estimates of error using out-of-bag (OOB) samples

Table 1
Land cover classes in the Castelporziano Natural Reserve with total "pure" area and inclusion/exclusion from classification.

Class code	Description	Area (ha)	Excluded from classification
C1	Water	0.81	X
C2	Agricultural land	445.23	
C3	Shrubland	31.14	
C4	Areas in recolonization	29.16	
C5	Special plantations	212.13	
C6	Pastures	82.44	
C7	Pastures with trees	37.17	
C8	Beach	31.95	
C9	Roads	1.62	X
C10	Urban areas	6.66	X
N1G	Mediterranean coniferous coastal dune forest	720.18	
S51	Mediterranean maquis and arborescent matorral	331.83	
T142	Mediterranean riparian *Populus* spp. forests	11.34	X
T195	Southeastern sub-thermophilous *Quercus* spp. forests	1627.29	
T19B6	Thermophilous *Fraxinus* spp. forests	21.6	
T211	*Quercus suber* forest	189.27	
T212	*Quercus ilex* and *Q. rotundifolia* forest	370.89	
	TOTAL	4150.71	

(Ahmed et al., 2022). Replicating the method applied in Vaglio Laurin et al. (2024), training and validation pixel selection for the Random Forest classifier involved random sampling within each EUNIS class, ensuring at least 250 pure PRISMA pixels (matching the size of the smallest class, T196B6—*Fraxinus* spp. forest). Seventy percent of the data (175 pixels) were randomly chosen for training the model and 30 % (75 pixels) for testing, apart from the aforementioned class, which had 168 pixels for training and 72 for testing (Vaglio Laurin et al., 2024). For S2 and PS, the pixels whose centroid fell inside the selected (250/240) PRISMA pixels were used for classification for three main reasons:

i) Minimize the impact of the selection of different training and validation sites among the three sensors on classification accuracy;
ii) Evaluate the influence of higher spatial resolution from the two multispectral sensors on classification outputs;
iii) Adopt a methodology similar to a ground-based study, utilizing fixed sample plots that contain varying numbers of satellite pixels based on the sensor used.

2.2. Input features for image classification

All the steps related to PRISMA and Sentinel 2 single date input features for classification are replicated from the previous work of Vaglio Laurin et al. (2024) over the same study area. The PRISMA classification utilized a single-date image acquired on 14 July 2022 to ensure optimal accuracy (evaluated against images from other dates in 2021 and 2022). Therefore, we report only the results from this best-performing single-date image. The downloaded image was co-registered with a yearly composite of S2, after which bands affected by noise or striping errors were removed (bands 1–9; 104–111; 148–164; 227–234), resulting in 192 usable bands.

For S2 and PS, the classification was performed using both single-date images—specifically from 14 July 2022 and 12 July 2022 (which was the closest available date to the PRISMA and S2 images) respectively—and median-based decadal (10-day) composites spanning the growing season from early March (Decade 6 of the year, hereafter abbreviated as D6) to the end of October 2022 (D30). The decadal composites for S2 and PS were derived from a varying number of images available for each decade, each having a maximum cloud cover of 20 %. Decade 25 is excluded due to the unavailability of cloud-free images for both sensors, while Decades 7, 11, 15, and 24 through 29 are missing for S2. For further details regarding the dates and the number of images used for each composite, refer to Table S1 (supplementary materials).

The Random Forest classification was performed using vegetation indices as predictors (see Table S2, supplementary materials). The use of vegetation indices has been shown in the scientific literature to provide a more robust understanding of ecosystem dynamics at the habitat scale (Bartold and Kluczek, 2024) and to contribute to the characterization of vegetation properties (Ahmed et al., 2022). A total of 28 indices were computed for PRISMA, while 22 indices were computed for S2 and 12 for PS. These indices were selected for their sensitivity to foliar chemical traits (e.g., the presence of specific photosynthetic pigments, nitrogen, water, lignin, and cellulose), which may vary at the species level due to different stoichiometric relationships (Asner and Martin, 2016).

All single-date images were treated uniformly (replicating Vaglio Laurin et al., 2024):

- Step 1: Identification of the top 10 most important indices. Each image underwent classification using all available indices. The top 10 indices were selected based on their Mean Decrease Accuracy (MDA) score, indicating their influence on classification accuracy (Benard et al., 2022; Breiman, 2001);
- Step 2: Reducing multicollinearity. Variance Inflation Factor (VIF) analysis, with a threshold of 5 (Girma et al., 2016), was applied to the top 10 indices to identify and remove highly correlated features using the *usdm* package in RStudio (Naimi et al., 2014). This ensured the development of statistically robust models (Ferré, 2009).

This process resulted in 6 remaining indices for PRISMA and 5 for S2 and PS.

For the S2 and PS 10-day composites, to reduce the high dimensionality of input predictors (12 indices * 16 decades for S2 and 24 decades for PS, totalling 192 and 288 layers, respectively), the VIF was computed directly on each decadal stack for each index. This initial step checked for temporal multicollinearity among layers representing the same index computed at different times during the growing season. The remaining layers after this first round of VIF were then stacked together, and VIF was re-evaluated to assess multicollinearity among the different indices. A final stack of 45 indices was obtained for S2 and 44 indices for PS. Given that this number of input features was still high compared to the number of classes (13), it could potentially lead to overfitting and excessive computational time (Hua et al., 2005; Kuhn and Johnson, 2013). Therefore, two alternative methods were applied to sieve and select spectral predictors from the temporal information contained in the stack: i) selecting the top two most important VIs by MDA score for each season (defined as winter, spring, summer, and fall based on 10-day composite dates), resulting in 8 VIs; and ii) applying a more restrictive VIF threshold (equal to 2 instead of 5), leaving 10 indices.

Data from a CHM of the Reserve was added to the input features, as the CHM provides information on the structural composition of the canopy, which may aid in distinguishing between vegetation types with similar reflectance but different structural properties (e.g., *Q. ilex* forest, T212, and maquis, S51, in the study area; Lang et al., 2023). The data were obtained from an airborne lidar survey conducted in 2007/2009, with a point density of 1.7 pulses per meter. The CHM was derived by calculating the difference between the Digital Elevation Model and the Digital Surface Model (Scrinzi et al., 2019; Vaglio Laurin et al., 2024). The data was originally at 1 m resolution and was resampled to 30 m, 10 m, and 3 m for the three sensors, respectively. Mean resampled values and standard deviations of the CHM were used as input features for the Random Forest model. Table 2 provides a list of input indices for the classification.

2.3. Classification procedure

All the steps related to PRISMA and Sentinel 2 single date classification are replicated from the previous work of Vaglio Laurin et al. (2024) over the same study area. We performed Random Forest classification on the seven datasets using RStudio version 2023.12.0 + 369, utilizing the *caret* (Kuhn, 2008) and *RandomForest* (Liaw and Wiener, 2002) packages. The number of trees (*ntree* parameter) was set to 500 for each classification, as literature indicates that this number stabilizes error (Belgiu and Drăgu, 2016). The number of splits at each node (*mtry*) was set to 2 for each single-date image and to 3 and 4 for the multi-date classifications involving 2 VIs per season and VIF < 2 for S2 and PS.

In addition to the hold-out validation method (70/30 split), 10-fold cross-validation was conducted for each classification model, as the estimate of prediction error is considered almost unbiased for $k = 10$ (Berrar, 2019; Simon, 2007). Cross-validation was implemented to mitigate the influence of autocorrelation between training and test sites, which represents a major drawback of this study design, particularly for classes covering smaller areas. This approach provides more robust estimates (Karasiak et al., 2022).

EUNIS Habitat Classification maps were generated in RStudio using the *predict* function from the *raster* package (Hijmans et al., 2015) for PRISMA and the best-performing classifications obtained from the two multispectral sensors. Additionally, probability maps were extracted for each of the seven habitat classes, with values ranging from 0 (no probability of the pixel being classified as the given class) to 1 (certainty of the pixel being classified as the given class) for each of the three best-performing datasets. The maps from the two multispectral sensors

Table 2
Spectral indices selected as input variables for the final classification (green). Decades for each index were added for the multi-date datasets.

Vegetation Indices	PRISMA	S2 single-date	PS single-date	S2 2 VIs per season	S2 VIF < 2	PS 2 VIs per season	PS VIF < 2
Anthocyanin Reflectance Index (ARI)				D6, D30			
Carotenoid Reflectance Index (CRI)				D22, D30		D7	
Cellulose Absorption Index (CAI)							
Enhanced Vegetation Index (EVI)					D6, D30		D7, D12, D26
Inverted Red-Edge Chlorophyll Index (IRECI)				D12			
Modified Chlorophyll Absorption Ratio Index (MCARI)						D28	
Photochemical Reflectance Index (PRI)				D18		D8, D16, D20, D21, D28	D9, D12, D20, D24, D27
Red-Edge Position (REP)					D6, D9, D10, D12, D14, D18, D23, D30		
Red-Green Ratio (RG)						D10	
Short Wave Infrared Ratio (SWIR)							
Simple ratio (SR NIR/R)							D7
Soil Adjusted Total Vegetation Index (SATVI)				D8			
Transformed Chlorophyll Absorption Ratio Index (TCARI)				D14			
Visible Atmospherically Resistant Index (VARI)							D7
Water Band Index (WBI)							
TOT indices as input variables	6	5	5	8	10	8	10

were resampled to PRISMA spatial resolution (30 m), and the three maps were combined to create a single map for each EUNIS habitat type, representing the average probability across the three sensors. This approach was employed to evaluate the combined performance of the three sensors in identifying the spatial patterns of different habitats and the associated degree of uncertainty, providing a visual assessment of classification errors. In contrast, confusion matrices offer a quantitative assessment of error (Xia and Lv, 2024).

Per-class variable importance was extracted using the *varImp* function from the *caret* package.

3. Results

3.1. Accuracy metrics

The results indicate that the PRISMA single-image dataset achieves the highest classification accuracy, with an Overall Accuracy (OA) of 84 %, as well as the highest User's Accuracy (UA) and Producer's Accuracy (PA) for almost all classes. The second-best results (OA = 75 %) were obtained from the S2 multi-date dataset utilizing only indices with a VIF score lower than 2. This is closely followed by the other multi-date

Table 3
Accuracy metrics of the seven classification datasets. OA = Overall Accuracy; UA = User Accuracy; PA = Producer Accuracy.

	PRISMA		S2 single-date		PS single-date		S2 2 VIs per season		S2 VIF < 2		PS 2 VIs per season		PS VIF < 2	
N. of input features	8		7		7		10		12		10		12	
OA	0.84		0.72		0.69		0.74		0.75		0.73		0.74	
Class	UA	PA	UA	PA	UA	PA	UA	PA	UA	PA	UA	PA	UA	PA
C2	0.92	0.87	0.82	0.76	0.75	0.73	0.86	0.77	0.92	0.82	0.83	0.78	0.94	0.83
C3	0.78	0.91	0.72	0.79	0.68	0.77	0.71	0.78	0.75	0.81	0.76	0.85	0.77	0.86
C4	0.92	0.96	0.91	0.97	0.89	0.94	0.94	0.96	0.95	0.97	0.96	0.95	0.95	0.95
C5	0.79	0.84	0.59	0.63	0.57	0.65	0.62	0.67	0.60	0.64	0.66	0.77	0.61	0.65
C6	0.84	0.88	0.71	0.74	0.71	0.68	0.76	0.74	0.77	0.84	0.78	0.81	0.79	0.84
C7	0.79	0.76	0.61	0.67	0.57	0.66	0.63	0.63	0.62	0.62	0.57	0.54	0.64	0.65
C8	1.00	1.00	1.00	1.00	0.99	0.99	0.99	0.99	1.00	1.00	0.99	1.00	1.00	1.00
N1G	0.79	0.88	0.80	0.88	0.76	0.78	0.81	0.85	0.79	0.87	0.74	0.72	0.71	0.66
S51	0.86	0.75	0.73	0.65	0.68	0.56	0.71	0.65	0.76	0.66	0.76	0.65	0.72	0.62
T195	0.87	0.69	0.65	0.56	0.56	0.38	0.65	0.63	0.57	0.55	0.55	0.41	0.56	0.50
T19B6	0.81	0.89	0.77	0.72	0.72	0.79	0.79	0.76	0.82	0.79	0.73	0.79	0.81	0.78
T211	0.75	0.75	0.44	0.43	0.45	0.52	0.55	0.57	0.59	0.59	0.54	0.62	0.54	0.63
T212	0.85	0.74	0.60	0.55	0.58	0.47	0.63	0.64	0.67	0.64	0.61	0.58	0.67	0.58

datasets, which yielded OAs ranging from 73 % to 74 %. The multispectral single-date datasets achieved OAs of 72 % for S2 and 69 % for PS. Table 3 presents the accuracy metrics for all seven classification datasets.

The single-date classification using the PRISMA image demonstrates the highest per-class accuracy across all classes, except for Agricultural Land (C2), where it is outperformed in UA by the PS multi-date classification utilizing indices with a VIF score lower than 2. For the forest classes, which are the focus of this study, the PRISMA single-image classification exhibits the highest accuracy for all classes, except for the Mediterranean conifers class (N1G), where the UA is slightly higher for the S2 single-image classification. Generally, in the single-date PRISMA classification, all forest classes exceed the 70 % accuracy threshold.

As for the four multi-date classifications, all outperform the single-date results from the multispectral datasets. In particular, the classifications using two VIs per season and those employing only indices with a VIF score lower than 2 show increases in overall accuracy of 4 % and 5 % for PS, and 2 % and 3 % for S2, compared to the single-date classifications.

Turning to the 10-fold cross-validation results (Table 4), the S2 classification using only indices with a VIF score lower than 2 reports the lowest out-of-bag (OOB) estimate of the error rate, as well as the lowest class-specific error for most land use types. The PRISMA single-date classification ranks as the second best-performing model, followed by PS using only indices with a VIF score lower than 2. All other classification datasets report OOB error estimates exceeding 20 %.

Fig. 2 presents the classification maps of the three datasets with the highest accuracy: the PRISMA single-date dataset and the multi-date datasets from S2 and PS, both utilizing only indices with a VIF score lower than 2 as input variables.

3.2. Confusion matrices

Tables 5–7 present the confusion matrices for the three highest-performing classification datasets.

In the case of PRISMA (Table 5), there is a misclassification between shrubland (C3) and maquis (S51), similar to the results observed for S2. Additionally, confusion arises between pine (N1G) and *Q. suber* (T211) stands. For both S2 and PS (Tables 6 and 7), the two evergreen oak habitats (T211 and T212) are frequently misclassified as each other. Furthermore, S2 misclassifies special plantations (C5) as *Q. suber* forest (T211), while PS shows confusion between *Q. suber* and maquis (S51). Across all datasets, the Mediterranean conifer forest (N1G) and *Fraxinus* spp. stands (T19B6) exhibit the lowest misclassification rates, followed by maquis (S51).

3.3. Variable importance

Fig. 3 presents the variable importance scores by class for the three highest-performing classification datasets.

In the case of PRISMA (Fig. 3a), the Transformed Chlorophyll Absorption Reflectance Index (TCARI; Haboudane et al., 2004), an indicator of chlorophyll abundance, is the most important predictor for three out of six forest classes: the pine stands (N1G) and the two evergreen Mediterranean oak types (T211 and T212). For the deciduous oak forest (T195) and ash stands (T19B6), the mean value of the CHM emerges as the most significant variable, as it does for areas undergoing recolonization (C4). For the maquis (S51), the standard deviation of the CHM is the most important predictor, followed by its mean.

In the best-performing S2 classification (Fig. 3b), the mean CHM value is the most important variable for classifying the ash stands (T19B6) and *Q. ilex* forest (T212). As in PRISMA, the standard deviation of the CHM is the primary predictor for the maquis (S51). For the other forest classes, the Enhanced Vegetation Index (EVI), computed using red, NIR, and blue wavelengths to correct for soil and atmospheric effects, and commonly used to quantify vegetation greenness (Huete et al., 2002), is essential for classifying the pine stands (N1G) in decade 6 (1–10 March). The Red-Edge Position (REP), an index sensitive to changes in chlorophyll concentration (Curran et al., 1995), is a key predictor for the deciduous oak forest (T195) in decades 10 (10–19 April) and 12 (30 April–9 May) for the *Q. suber* stands (T211).

In the PS multi-date classification utilizing only indices with a VIF score lower than 2 (Fig. 3c), the mean CHM value is the most important predictor for three out of six habitat types: the pine stands (N1G), maquis (S51), and *Q. ilex* forest (T212). The EVI from decade 12 (30 April–9 May) is the most significant variable for distinguishing the deciduous oak forest (T195) and ash stands (T19B6), closely followed in both cases by the same index from decade 26 (17–26 September). For the *Q. suber* habitat (T211), the Simple Ratio (SR) from decade 7 (11–20 March) is the primary predictor, closely followed by the mean CHM.

3.4. Forest classes

Fig. 4 presents the combined probability maps of the three highest-performing classification datasets for each of the seven forest classes present in the Reserve. As illustrated in the maps, the deciduous oak forest class (T195; Fig. 4c) exhibits the highest proportion of pixels with significant uncertainty, specifically within the probability percentage classes of 21–40 % and 41–60 %. The *Q. suber* forest class (T211; Fig. 4e) also displays a considerable number of uncertain pixels compared to other categories. Conversely, the *P. pinea* class (N1G; Fig. 4a) and the maquis (S51; Fig. 4b) contain a greater number of pixels with lower (1–20 %) and higher (61–80 % and 81–100 %) classification probability

Table 4
10-fold cross-validation results for the seven classification datasets.

	PRISMA	S2 single-date	PS single-date	S2 2 VIs per season	S2 VIF < 2	PS 2 VIs per season	PS VIF < 2
OOB estimate of error rate	17.79 %	26.74 %	28.84 %	25.26 %	16.68 %	21.16 %	19.08 %
Class	Classification error						
C2	0.15	0.24	0.26	0.26	0.15	0.17	0.13
C3	0.13	0.23	0.25	0.24	0.14	0.16	0.15
C4	0.05	0.06	0.06	0.06	0.05	0.06	0.03
C5	0.21	0.36	0.35	0.37	0.25	0.21	0.25
C6	0.14	0.25	0.25	0.23	0.10	0.11	0.09
C7	0.23	0.28	0.30	0.42	0.24	0.32	0.24
C8	0.00	0.00	0.01	0.00	0.00	0.00	0.00
N1G	0.15	0.12	0.19	0.16	0.10	0.24	0.28
S51	0.21	0.27	0.30	0.26	0.19	0.20	0.23
T195	0.38	0.38	0.59	0.32	0.27	0.41	0.32
T19B6	0.14	0.30	0.21	0.30	0.17	0.22	0.18
T211	0.27	0.57	0.49	0.35	0.26	0.35	0.27
T212	0.26	0.43	0.48	0.34	0.24	0.34	0.36

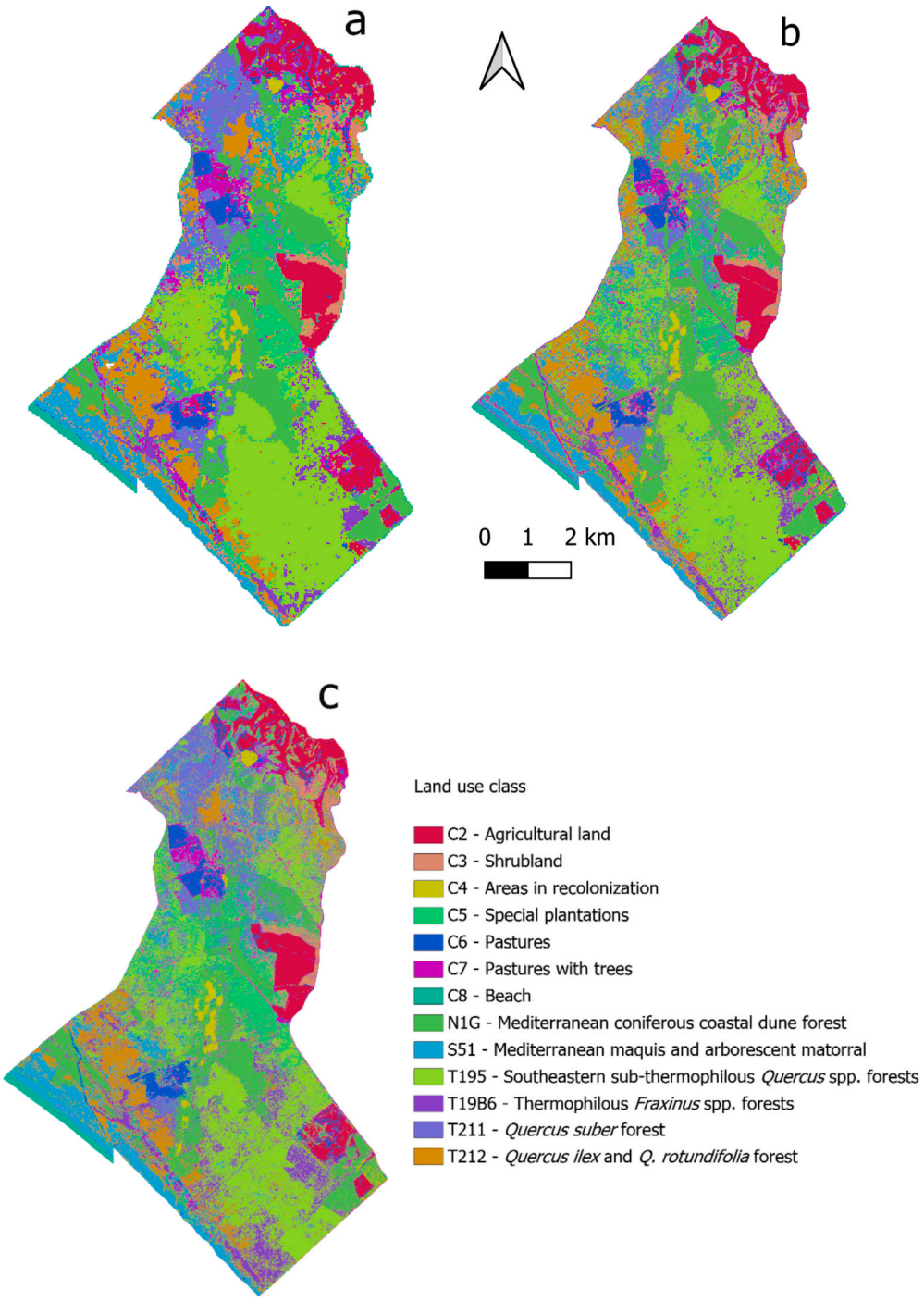


Fig. 2. Classification maps of the three best classification datasets: a) PRISMA single-date; b) multi-date Sentinel-2 using only indices with VIF score < 2; c) multi-date PlanetScope using only indices with VIF score < 2.

rates.

4. Discussion

4.1. Accuracy metrics and variable importance

As previously demonstrated by Vaglio Laurin et al. (2024), PRISMA achieved the highest overall accuracy, exceeding 80 % (Table 3), thereby corroborating the findings of Vaglio Laurin et al. (2024). All classes exceeded a 70 % accuracy threshold, successfully differentiating between tree species within the same genus, such as *Q. suber* (T211) and *Q. ilex* (T212). Notably, the single-date S2 dataset, also previously tested in Vaglio Laurin et al. (2024), outperformed PS by approximately 3 %. Utilizing multi-date data with a VIF score lower than 2 yielded enhanced results for both multispectral sensors, with accuracy improvements of 2–3 % for S2 and 4–5 % for PS compared to their single-date counterparts. Given the considerable number of classes, the three best classification results can be regarded as satisfactory, with Overall Accuracy scores ranging from 75 % to 80 %, aligning with the proposed range by Pesaresi et al. (2022) for cases with more than five classes.

The analysis of the 10-fold cross-validation results (Table 4) reaffirms the advantage of multi-date classification. Among all methods, S2

Table 5
Confusion matrix of the PRISMA single-date classification dataset; columns are reference, rows are predicted values. Correctly classified pixels are highlighted in green.

	C2	C3	C4	C5	C6	C7	C8	N1G	S51	T195	T19B6	T211	T212
C2	65	0	0	0	4	2	0	0	0	0	0	0	0
C3	0	68	0	3	0	2	0	0	9	4	0	0	1
C4	0	0	72	0	0	3	0	2	0	0	1	0	0
C5	0	4	0	63	0	0	0	0	3	6	1	0	3
C6	9	0	0	0	66	4	0	0	0	0	0	0	0
C7	0	0	1	1	5	57	0	2	0	0	3	2	1
C8	0	0	0	0	0	0	75	0	0	0	0	0	0
N1G	0	0	0	1	0	3	0	66	0	0	0	11	3
S51	0	2	0	0	0	0	0	0	56	1	0	4	2
T195	0	0	0	4	0	0	0	1	0	52	1	0	2
T19B6	1	0	2	1	0	4	0	0	0	5	67	0	3
T211	0	1	0	0	0	0	0	4	6	4	0	56	4
T212	0	0	0	2	0	0	0	0	1	3	2	2	55

Table 6
Confusion matrix of the Sentinel-2 classification dataset using indices with VIF value <2; columns are reference, rows are predicted values. Correctly classified pixels are highlighted in green.

	C2	C3	C4	C5	C6	C7	C8	N1G	S51	T195	T19B6	T211	T212
C2	531	1	0	2	21	18	0	0	1	0	0	0	1
C3	5	546	0	26	5	28	0	4	66	18	12	9	12
C4	0	0	642	4	2	16	0	8	0	0	2	0	0
C5	1	16	1	432	1	37	0	5	31	59	14	90	31
C6	66	7	6	0	565	81	1	5	4	0	0	0	3
C7	37	16	9	34	75	420	2	22	12	4	12	18	13
C8	0	0	0	0	0	1	662	0	0	0	0	0	0
N1G	0	21	4	13	3	16	0	521	2	15	2	36	26
S51	1	34	0	2	0	3	0	1	443	38	5	40	14
T195	1	13	0	45	0	16	0	6	30	301	42	18	59
T19B6	2	11	0	3	1	24	0	7	0	49	535	4	14
T211	1	4	0	106	1	11	0	16	33	29	9	397	68
T212	3	6	2	8	1	4	0	3	53	30	42	63	434

Table 7
Confusion matrix of the PlanetScope classification dataset using indices with VIF value <2; columns are reference, rows are predicted values. Correctly classified pixels are highlighted in green.

	C2	C3	C4	C5	C6	C7	C8	N1G	S51	T195	T19B6	T211	T212
C2	3834	8	16	7	315	333	10	18	25	4	18	8	16
C3	34	5186	2	187	24	290	2	55	464	374	46	94	54
C4	2	0	5024	12	20	109	0	32	0	4	8	2	3
C5	1	278	16	4635	6	83	0	366	152	499	39	533	407
C6	623	18	31	0	4724	558	2	18	21	2	24	24	20
C7	276	83	100	57	651	2574	1	57	102	172	44	288	100
C8	0	0	0	0	3	0	6046	1	71	0	0	0	1
N1G	3	68	64	199	0	26	0	2918	0	69	83	245	274
S51	15	192	1	30	19	61	14	20	3879	250	82	261	269
T195	52	148	6	318	28	136	0	63	205	2073	295	101	339
T19B6	42	17	15	15	5	175	0	82	30	1124	4823	99	183
T211	15	42	21	411	60	387	0	112	721	228	187	3660	874
T212	44	35	11	123	12	70	0	304	324	241	426	598	3454

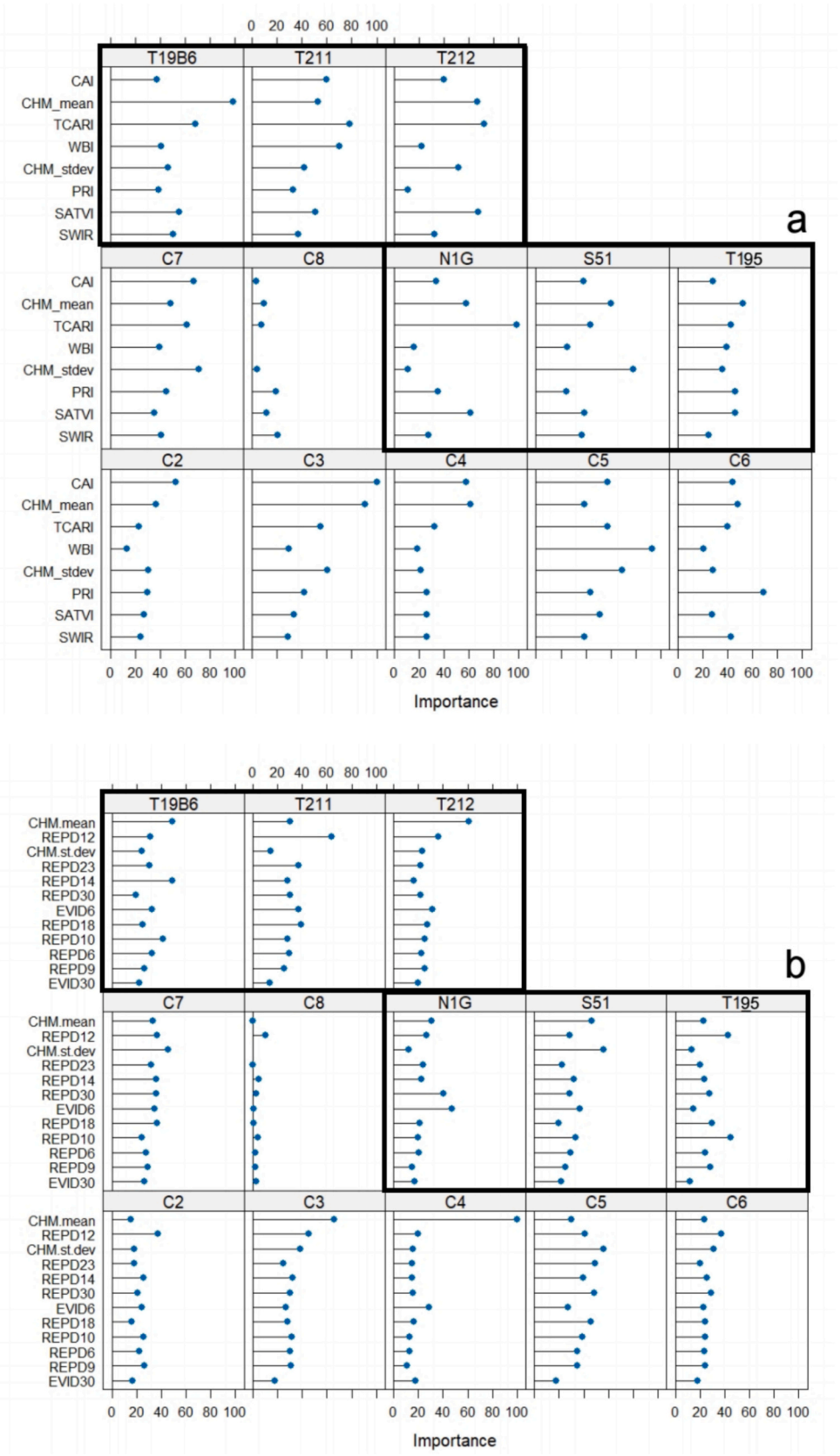


Fig. 3. Per-class variable importance of the three best classification datasets. a) PRISMA single-date; b) Sentinel-2 multi-date using only predictors with VIF score < 2; c) PlanetScope multi-date using only predictors with VIF score < 2. EUNIS habitat classes are highlighted with black boxes.

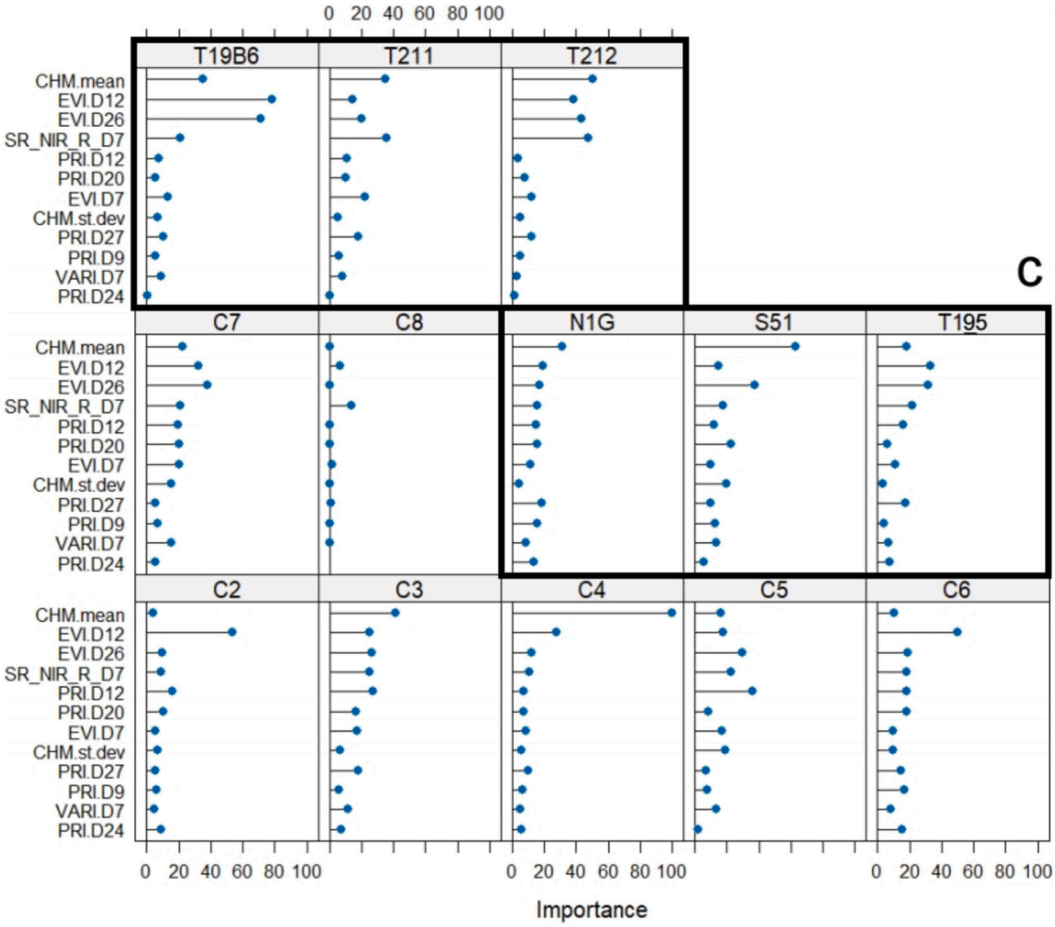


Fig. 3. (*continued*).

utilizing multi-date data and VIF filtering (VIF < 2), achieved the lowest Out-of-Bag (OOB) error rate of 16.68 %, outperforming PRISMA (17.79 %). In contrast, PS, using the same criteria, exhibited a higher OOB error than both S2 and PRISMA, although it remained below 20 %.

Focusing on forest habitats, S2 classification showed lower per-class error rates than PRISMA for all classes except for ash stands (T19B6), with all class errors remaining below 30 %. For the deciduous oak forest class (T195), PS also reported a lower class error compared to PRISMA. This suggests that employing cross-validation techniques with a higher number of available images across the growing season may reduce the overall confusion rate among classes. These findings further affirm the potential of multi-date S2 for habitat mapping, owing to the sensor's superior temporal resolution, availability, and spectral range across the visible, near-infrared (NIR), and short-wave infrared (SWIR) spectra. Previous studies have underscored these advantages (Arasumani et al., 2024; Marcinkowska-Ochtyra et al., 2023; Marzialetti et al., 2019; Pesaresi et al., 2022; Rapinel et al., 2019; Torresani et al., 2019), emphasizing the utility of the multi-temporal aspect when utilizing vegetation indices as input features (Le Dez et al., 2021), which was the approach taken in this study. The results obtained with S2 ultimately confirm the conclusions of Torresani et al. (2019) and Bartold and Kluczek (2024), highlighting the benefits of this sensor concerning acquisition costs (given that the dataset is entirely open-source), as well as spatial and temporal coverage in comparison to currently available hyperspectral sensors.

Among the three top-performing classifications (Fig. 3), the mean CHM emerged as a crucial predictor for multiple forest types across all sensors. It was identified as the most important variable for 2–3 classes within each sensor (PRISMA: T195 and T19B6; S2: T19B6 and T212; PS: N1G, S51, and T212). Additionally, the standard deviation of the CHM served as the primary predictor for the maquis (S51) in the PRISMA classification. These findings highlight the significance of the CHM, which provides insights into the variability of canopy height and vegetation structure, facilitating the differentiation of habitats with similar spectral reflectance (i.e., the maquis and evergreen Mediterranean oaks) based primarily on their structural properties.

The TCARI is a key predictor for several classes (N1G, T211, T212) and remains relevant for others (T19B6, S51) in the PRISMA classification (Fig. 3a). While TCARI can be calculated from all sensor data, it only appears as a significant variable within the PRISMA dataset. This limitation complicates the isolation of hyperspectral resolution's specific influence on TCARI's significance for classification accuracy, as the remaining variables after applying the VIF threshold likely also contribute to the final classification output. Furthermore, the PRISMA dataset uniquely provides two indices that necessitate a hyperspectral instrument: the Chlorophyll Absorbance Index (CAI) and the Water Band Index (WBI). These indices, which are not available for multispectral sensors, yield information on cellulose absorption (Daughtry et al., 2004) and leaf water content (Peñuelas et al., 1993), respectively. Notably, both CAI and WBI are important for most forest classes (Fig. 3a), particularly for the *Q. suber* forest (T211), where they rank as the second (WBI) and third (CAI) most important predictors after TCARI. Their significance may be attributed to the specific acquisition date of the PRISMA image, which coincided with one of the driest periods in the Mediterranean region (mid-July). During this period, SWIR wavelengths are particularly sensitive to variations in canopy water content.

The predominance of indices computed from spring images among the most important variables for the two multi-date classifications in the

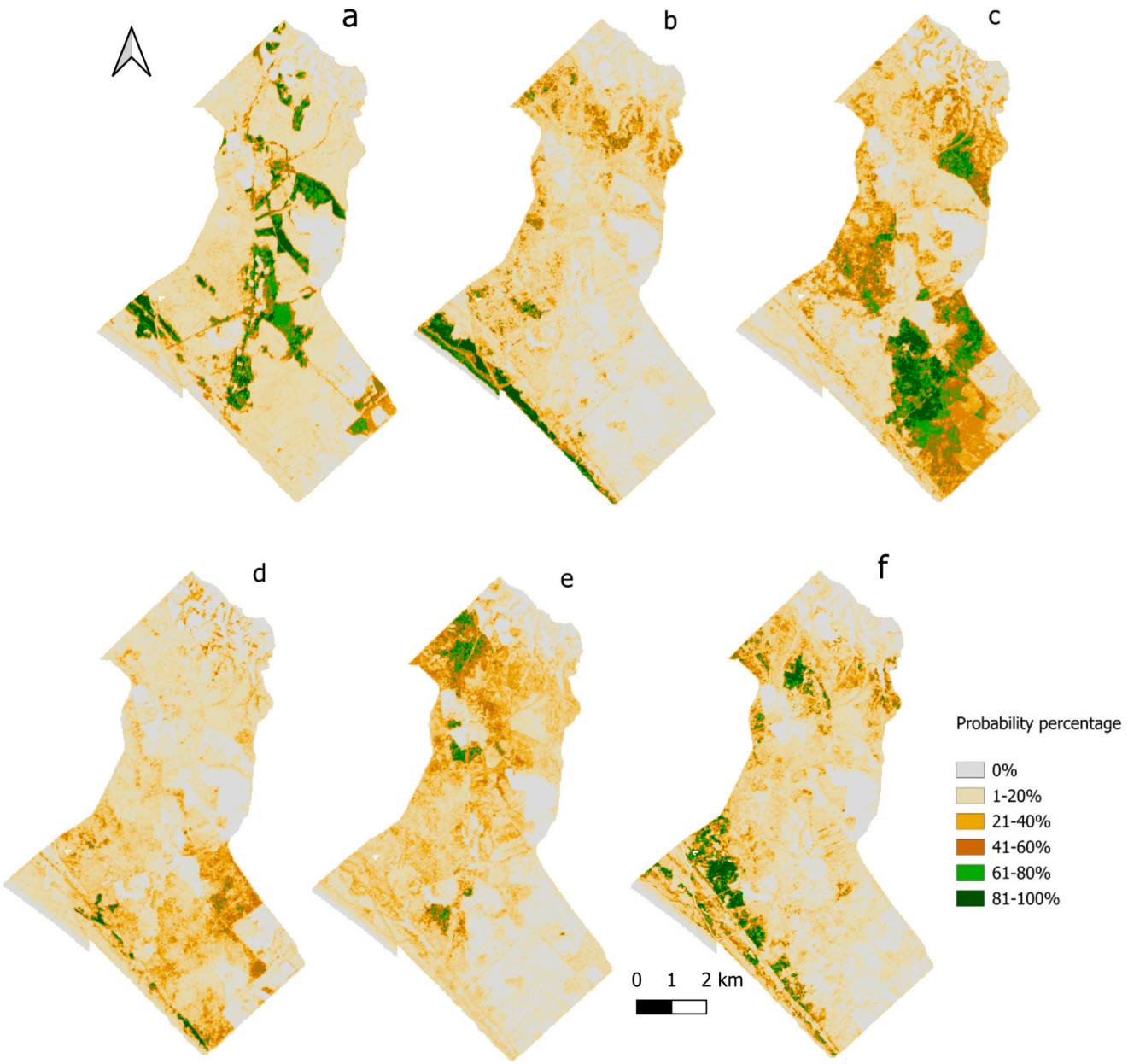


Fig. 4. Merged maps of the three best classification datasets for the seven forest types considered in the study; a) Mediterranean coniferous coastal dune forest (N1G); b) Mediterranean maquis and arborescent matorral (S51); c) Southeastern sub-thermophilous Quercus spp. forest (T195); d) Thermophilous Fraxinus spp. forest (T19B6); e) *Q. suber* forest (T211); f) *Q. ilex* and *Q. rotundifolia* forest (T212). Each map is accompanied by a histogram reporting the number of pixels in each probability percentage class.

case of S2 and PS (Fig. 3b and c) and good results (>80 % OA, Table 3) obtained from the single-date summer PRISMA image are consistent with previous studies identifying spring and summer as the times of the year (TOY) exhibiting the highest reflectance variation among different vegetation types, attributed to a more pronounced expression of pigment content during these times, which favours habitat discrimination (Arasumani et al., 2024; Le Dez et al., 2021; Torresani et al., 2019). Consequently, when mapping specific vegetation communities for management and conservation purposes, imagery acquired during these TOYs, alongside indices or wavelengths linked to water content, vegetation health, and photosynthetic activity (Rocchini et al., 2021), such as those in the red-edge, NIR, and SWIR spectra, could prove effective—especially in regions with seasonal phenology similar to that of the study area. These findings ultimately underscore the capacity of multi-temporal multispectral data to capture changes in vegetation phenology, as noted by Meerdink et al. (2024), revealing their potential as a powerful tool for habitat classification and biodiversity monitoring when combined with hyperspectral technology, as suggested by Vanguri et al. (2024).

4.2. *EUNIS habitats classification accuracy*

Across all datasets (Table 3), the deciduous oak forest (T195) and the *Q. suber* stands (T211) exhibit the lowest classification accuracies, a finding corroborated by the classification probability maps (Fig. 4c and e). The lower performance of the satellites for the deciduous oak forest may be attributed to its senescent phase, characterized by a lack of regeneration. This situation is exacerbated by excessive herbivory pressure on seedlings from fauna (Recanatesi et al., 2020; Scrinzi et al., 2016) and the adverse effects of saltwater intrusion (Capelli et al.,

2007), complicating the classification of this habitat type. Moreover, T195 is the most extensive category among those considered, leading to greater internal variability. The variation of spectral signatures within the same species or habitat type is not investigated in this study but warrants further exploration in future research, as already suggested by Vanguri et al. (2024).

Another significant limitation, emphasized by Meerdink et al. (2024), is that machine learning approaches are typically not designed to handle training data that is not "pure" and representative of a specific target species or canopy cover. For this reason, only randomly extracted pure pixels were employed as training data for the model. However, the extent of this habitat class and its intrinsic characteristics may render this approach suboptimal.

This case underscores the importance of mapping uncertainty (Rocchini et al., 2010), as demonstrated both visually (Fig. 4) and quantitatively (Tables 5–7) in this study. It highlights the need for caution when managing vegetation communities that occupy larger areas or are impacted by other factors, as their mapping can be complex. In this context, the value of employing different optical data sources, as previously stated by Vanguri et al. (2024), is also evident in this study. Such sources can provide a more robust foundation for identifying areas with a higher degree of certainty.

Examining the confusion matrices for the three best datasets (Tables 5–7), it is evident that the deciduous oak forest category is primarily misclassified as special plantations (C5), ash stands (T19B6), and *Q. ilex* forest (T212). In the case of PRISMA, misclassification also occurs with *Q. suber* (T211) and maquis (S51) for the two multispectral sensors. The spectral similarity in leaf reflectance between broadleaf species, such as *Fraxinus* spp., contributes to confusion in classification. Additionally, the senescent oak canopy may create open spaces that facilitate the growth of Mediterranean understory vegetation, further complicating classification. The category of special plantations, which includes agroforestry structures historically established within the Reserve, consists of planted, regular rows of either *Q. suber* or *Eucalyptus* spp., the latter causing misclassification in S2 and PS.

For *Q. suber*, the primary misclassification occurs with the maquis (S51) and *Q. ilex* (T212), due to the spectral similarities among these three categories. Notably, PRISMA is the only sensor to achieve and exceed the 70 % accuracy threshold in all three classes, underscoring the potential of hyperspectral data in distinguishing spectrally similar categories. The two multispectral sensors demonstrate a high degree of confusion between this class and special plantations (C5), paralleling the confusion observed in the deciduous oak forest (T195). This comparison with PRISMA reaffirms the notion that a broader spectral range enhances classification at the habitat level (Rocchini et al., 2010). Additionally, it indicates that higher spatial resolution is not invariably advantageous (Ghosh et al., 2014; Meerdink et al., 2024; Vangi et al., 2021), as increased spatial resolution can lead to greater internal variability within the same class, consequently reducing classification accuracy when employing per-pixel methods (Rocchini et al., 2010; Warren et al., 2014), as was observed in this study. The pixel-based approach may represent a limitation when utilizing high-resolution imagery such as PS. Therefore, exploring an object-based classification method, as implemented by Strasser and Lang (2015) or Abbas et al. (2020) with other optical imagery datasets, could be a viable alternative worth investigating.

Conversely, the *Fraxinus* spp. forest (T19B6) is the most accurately classified habitat, surpassing 70 % accuracy in all seven datasets. It is followed by the *P. pinea* forest (N1G), which achieves this threshold in all classifications except for the PS multi-date dataset employing only vegetation indices with VIF scores <2. Generally, PS reports lower accuracy for each class across all datasets compared to S2 and PRISMA. The limited extent of the *Fraxinus* spp. forest within the Castelporziano Natural Reserve facilitates its accurate detection, particularly since all pixels from this class were utilized for either training or testing the model, suggesting an underlying spatial autocorrelation. Regarding the *P. pinea* stands, they are easily identifiable, as there are no other vegetation communities within the Reserve that are taxonomically or spectrally similar, especially considering that as of summer 2022, most of these standing trees are dead due to phytosanitary issues (Recanatesi et al., 2019).

The inclusion of the CHM significantly aids in differentiating between *Q. ilex* stands (T212) and the maquis (S51), as vegetation height, rather than species composition, serves as the primary discriminant between Mediterranean forests and shrublands. In this context, the availability of lidar-derived metrics for the complete forest profile (i.e., the distribution of lidar returns at various heights) could assist in detecting forest strata and understory presence (Venier et al., 2019). Although this study did not account for such metrics, they could be crucial for monitoring the impacts of climate change on vegetation (Peñuelas and Sardans, 2021), as previously recommended by Vaglio Laurin et al. (2024).

The maquis (S51) is predominantly misclassified by the two multispectral sensors as either the two evergreen oak formations (*Q. suber*, T211; *Q. ilex*, T212) or as shrubland (C3). The structural composition and reflectance properties of shrubland can closely resemble those of the maquis, leading to confusion between the two. Regarding the confusion with the deciduous oak forest (T195), as previously discussed, this further illustrates that the senescent forest structure, lacking regeneration, creates openings for the establishment of Mediterranean shrubland.

5. Conclusion

This study evaluated the trade-off between spectral, spatial, and temporal resolutions of different sensors, testing multispectral Sentinel-2 and PlanetScope imagery and comparing the results with those obtained in a previous study with single-date PRISMA hyperspectral and Sentinel-2 sensors, in the context of classifying EUNIS level 3 habitats in the Castelporziano Natural Reserve. Utilizing spectral indices and Random Forest algorithms, the research was conducted in a challenging test site characterized by diverse forest types with similar reflectance and structural properties.

Confirming previous results from Vaglio Laurin et al. (2024), the present findings suggest that the wider spectral ranges and narrower bands of hyperspectral sensors like PRISMA may partially mitigate the limitations posed by infrequent temporal observations. Furthermore, the study identifies critical periods and spectral regions for habitat mapping in areas exhibiting similar seasonal phenology to the Castelporziano Natural Reserve. Specifically, data collected in spring and summer, particularly in the red and green wavelengths, proved essential for canopy cover discrimination across all datasets. Additionally, the red-edge region was particularly informative for the Sentinel-2 multi-date classifications, while SWIR wavelengths significantly contributed to classification accuracy within the PRISMA dataset.

To our knowledge, this is the first comprehensive comparison of the spectral, spatial, and temporal characteristics of these three recently launched sensors, investigating their influence on classification accuracy. Our findings underscore the importance of integrating data from diverse sources for more robust forest habitat mapping, thereby supporting management and conservation initiatives. An advisable strategy may involve utilizing hyperspectral imagery as an initial classification "filter" (Rocchini et al., 2010; Torresani et al., 2019), followed by employing the denser S2 time series for monitoring seasonal changes. Conversely, PS data may be more suited for finer-scale monitoring due to its higher spatial resolution and daily coverage, facilitating timely assessments of changes in smaller areas after broader-scale habitat type delineation. Alternatively, implementing an object-based classification approach for PS data could mitigate the limitations associated with the pixel-based method employed in this study. This combined approach could enhance efficiency and reduce the subjectivity, costs, and time required for traditional habitat mapping methods, such as field surveys

(Rocchini et al., 2021; Strasser and Lang, 2015; Warren et al., 2014).

Moreover, the integration of a Canopy Height Model proved essential for distinguishing between habitat types that exhibit similar reflectance but differ structurally, such as maquis and *Q. ilex* forest. Utilizing LiDAR data across various heights could provide even richer information, enabling subtyping based on understory composition—an aspect critical for monitoring habitats and conserving complex ecosystems. Although this approach falls beyond the scope of the current study, it merits further exploration in future research.

This investigation into forest habitat classification was conducted within a Mediterranean protected area featuring relic formations. To assess the generalizability of our methodology, it would be valuable to replicate this study in other critical conservation sites across diverse climatic and geographic contexts. Such efforts would allow us to evaluate the feasibility of our approach in various habitats and observe potential variations in classification outcomes across different ecosystems.

CRediT authorship contribution statement

Chiara Zabeo: Writing – original draft, Visualization, Methodology, Investigation, Formal analysis. **Gaia Vaglio Laurin:** Writing – review & editing, Supervision, Methodology, Formal analysis, Conceptualization. **Birhane Gebrehiwot Tesfamariam:** Formal analysis. **Diego Giuliarelli:** Methodology, Data curation. **Riccardo Valentini:** Supervision. **Anna Barbati:** Writing – review & editing, Supervision, Methodology.

Declaration of generative AI and AI-assisted technologies in the writing process

During the preparation of this work the authors used Grammarly and ChatGPT to improve spelling, grammar and conciseness of the English language in the manuscript. After using these tools, the authors reviewed and edited the content as needed and take full responsibility for the content of the publication.

Declaration of competing interest

The authors declare the following financial interests/personal relationships which may be considered as potential competing interests:

Gaia Vaglio Laurin reports financial support was provided by Italian Space Agency. Chiara Zabeo reports financial support was provided by Ministry of Education and Merit. If there are other authors, they declare that they have no known competing financial interests or personal relationships that could have appeared to influence the work reported in this paper.

Data availability

The data supporting this study's findings are openly available at https://figshare.com/articles/dataset/Habitat_Mapping_Castelporziano/27269778?file=49899582, including the codes, shapefiles, and Sentinel-2 data used.

Due to legal and commercial reasons, the PRISMA and PlanetScope data are not available for sharing. PRISMA satellite images are accessible from the mission official website https://prisma.asi.it (last accessed on 22 October 2024) upon approval of a formal data request to the Italian Space Agency, while PlanetScope data are accessible from Planet's official website https://www.planet.com/ (last accessed on 22 October 2024) upon contract.

Acknowledgements

This work was supported by the Italian Space Agency (ASI) research grant "HYPERECOS - Hyperspectral Prisma Data for Ecosystem functions, habitats, and diversity characterization", CUP: F83C22000440005, and by the Italian Ministry of Education and Merit (MIUR) through the PRIN 2020 "MULTIFOR - Multi-scale observations to predict Forest response to pollution and climate change", CUP: B83C22001580005.

The authors acknowledge Planet Labs for providing access to the satellite images used in this study through the Education and Research program (https://www.planet.com/industries/education-and-research/).

GVL acknowledges the PNRR, Missione 4, Componente 2, Avviso 3264/2021, IR0000032—ITINERIS—Italian Integrated Environmental Research Infrastructures System CUP: B53C22002150006.

AB acknowledges the National Recovery and Resilience Plan (NRRP), Missione 4, Componente 2, Call for Tender 3138/2021: Project code CN_00000033 National Biodiversity Future Center – NBFC CUP: J83C22000860007.

The authors acknowledge the support of Dr. Daniele Cecca, Vice Director of the Castelporziano Natural Reserve.

Appendix A. Supplementary data

Supplementary data to this article can be found online at https://doi.org/10.1016/j.ecoinf.2024.102867.

References

Abbas, S., Nichol, J.E., Wong, M.S., 2020. Object-based, multi-sensor habitat mapping of successional age classes for effective management of a 70-year secondary forest succession. Land Use Policy 99, 103360. https://doi.org/10.1016/J.LANDUSEPOL.2018.04.035.

Aditya, M.A., Milind, S., Robin, B.V.V., Arasumani, M., Robin, V.V., Singh, A., Bunyan, M., 2021. Testing the efficacy of hyperspectral (AVIRIS-NG), multispectral (Sentinel-2) and radar (Sentinel-1) remote sensing images to detect native and invasive non-native trees. Biol. Invasions 23, 2863–2879. https://doi.org/10.1007/s10530-021-02543-2.

Ahmed, N., Atzberger, C., Zewdie, W., 2022. The potential of modeling *Prosopis Juliflora* invasion using Sentinel-2 satellite data and environmental variables in the dryland ecosystem of Ethiopia. Eco. Inform. 68, 101545. https://doi.org/10.1016/J.ECOINF.2021.101545.

Amieva, J.F., Oxoli, D., Brovelli, M.A., 2023. Machine and deep learning regression of chlorophyll-a concentrations in lakes using PRISMA satellite hyperspectral imagery. Remote Sens. 15 (22). https://doi.org/10.3390/rs15225385.

Arasumani, M., Thiel, F., Pham, V.D., Hellmann, C., Kaiser, M., van der Linden, S., 2023. Advancing peatland vegetation mapping by spaceborne imaging spectroscopy. Ecol. Indic. 154. https://doi.org/10.1016/J.ECOLIND.2023.110665.

Arasumani, M., Kumaresan, M., Esakki, B., 2024. Mapping native and non-native vegetation communities in a coastal wetland complex using multi-seasonal Sentinel-2 time series. Biol. Invasions 26 (4), 1105–1124. https://doi.org/10.1007/S10530-023-03232-Y.

ASI, 2020. PRISMA Products Specification Document Issue 2.1 Date 12/02/2020.

Asner, G.P., Martin, R.E., 2016. Spectranomics: emerging science and conservation opportunities at the interface of biodiversity and remote sensing. Glob. Ecol. Conserv. 8, 212–219. https://doi.org/10.1016/j.gecco.2016.09.010.

Bartold, M., Kluczek, M., 2024. Estimating of chlorophyll fluorescence parameter Fv/Fm for plant stress detection at peatlands under Ramsar convention with Sentinel-2 satellite imagery. Eco. Inform. 81, 102603. https://doi.org/10.1016/J.ECOINF.2024.102603.

Bayle, A., Carlson, B.Z., Thierion, V., Isenmann, M., Choler, P., 2019. Improved mapping of mountain Shrublands using the Sentinel-2 red-edge band. Remote Sens. 11 (23), 2807. https://doi.org/10.3390/RS11232807.

Begliomini, F.N., Barbosa, C.C.F., Martins, V.S., Novo, E.M.L.M., Paulino, R.S., Maciel, D. A., Lima, M.A., O'shea, R.E., Pahlevan, N., Lamparelli, M.C., 2023. Machine learning for cyanobacteria mapping on tropical urban reservoirs using PRISMA hyperspectral data ISPRS Journal of photogrammetry and remote sensing. ISPRS J. Photogramm. Remote Sens. 204, 378–396. https://doi.org/10.1016/j.isprsjprs.2023.09.019.

Belgiu, M., Drăgu, L., 2016. Random forest in remote sensing: a review of applications and future directions. ISPRS J. Photogramm. Remote Sens. 114, 24–31. https://doi.org/10.1016/J.ISPRSJPRS.2016.01.011.

Benard, C., Da Veiga, S., Scornet, E., 2022. Mean decrease accuracy for random forests: inconsistency, and a practical solution via the Sobol-MDA. Biometrika 109 (4), 881–900. https://doi.org/10.1093/BIOMET/ASAC017.

Berrar, D., 2019. Cross-Validation. Encyclopedia of Bioinformatics and Computational Biology: ABC of Bioinformatics, 1–3, pp. 542–545. https://doi.org/10.1016/B978-0-12-809633-8.20349-X.

Breiman, L., 2001. Random Forests, 45, pp. 5–32.

Capelli, G., Mazza, R., Papiccio, C., 2007. Intrusione salina nel Delta del Fiume Tevere. Geologia, idrologia e idrogeologia del settore romano della piana costiera. Giornale Di Geologia Applicata 5, 13–28. https://doi.org/10.1474/GGA.2007-05.0-02.0171.

Cavender-Bares, J., Meireles, J.E., Couture, J.J., Kaproth, M.A., Kingdon, C.C., Singh, A., Serbin, S.P., Center, A., Zuniga, E., Pilz, G., Townsend, P.A., Ustin, S.L., Roy, S., Thenkabail, P.S., 2016. Associations of leaf spectra with genetic and phylogenetic variation in oaks: prospects for remote detection of biodiversity. Remote Sens. 8 (3), 221. https://doi.org/10.3390/rs8030221.

Chytrý, M., Tichý, L., Hennekens, S.M., Knollová, I., Janssen, J.A.M., Rodwell, J.S., Peterka, T., Marcenò, C., Landucci, F., Danihelka, J., Hájek, M., Dengler, J., Novák, P., Zukal, D., Jiménez-Alfaro, B., Mucina, L., Abdulhak, S., Aćić, S., Agrillo, E., Schaminée, J.H.J., 2020. EUNIS habitat classification: expert system, characteristic species combinations and distribution maps of European habitats. Appl. Veg. Sci. 23 (4), 648–675. https://doi.org/10.1111/avsc.12519.

Cogliati, S., Sarti, F., Chiarantini, L., Cosi, M., Lorusso, R., Lopinto, E., Miglietta, F., Genesio, L., Guanter, L., Damm, A., Pérez-López, S., Scheffler, D., Tagliabue, G., Panigada, C., Rascher, U., Dowling, T.P.F., Giardino, C., Colombo, R., 2021. The PRISMA imaging spectroscopy mission: overview and first performance analysis. Remote Sens. Environ. 262. https://doi.org/10.1016/j.rse.2021.112499.

Coppo, P., Brandani, F., Faraci, M., Sarti, F., Cosi, M., 2019. Leonardo Spaceborne Infrared Payloads for Earth Observation: SLSTRs for Copernicus Sentinel 3 and PRISMA Hyperspectral Camera for PRISMA Satellite, 1. https://doi.org/10.3390/proceedings2019027001.

Curran, P.J., Windham, W.R., Gholz, H.L., 1995. Exploring the relationship between reflectance red edge and chlorophyll concentration in slash pine leaves. Tree Physiol. 15 (3), 203–206. https://doi.org/10.1093/TREEPHYS/15.3.203.

Daughtry, C.S.T., Hunt, E.R., McMurtrey, J.E., 2004. Assessing crop residue cover using shortwave infrared reflectance. Remote Sens. Environ. 90 (1), 126–134. https://doi.org/10.1016/J.RSE.2003.10.023.

de Abreu Araújo, J., Galvão, L.S., Dalagnol, R., 2023. Sensitivity of hyperspectral vegetation indices to rainfall seasonality in the Brazilian savannahs: an analysis using PRISMA data. Remote Sens. Lett. 14 (3), 277–287. https://doi.org/10.1080/2150704X.2023.2189031.

de Lima, T.M.A., Giardino, C., Bresciani, M., Barbosa, C.C.F., Fabbretto, A., Pellegrino, A., Begliomini, F.N., 2023. Assessment of estimated Phycocyanin and chlorophyll-a concentration from PRISMA and OLCI in Brazilian inland waters: a comparison between semi-analytical and machine learning algorithms. Remote Sens. 15 (5). https://doi.org/10.3390/rs15051299.

D'odorico, P., Schuman, M.C., Kurz, M., Csilléry, K., 2023. Discerning oriental from European beech by leaf spectroscopy: operational and physiological implications. For. Ecol. Manag. 541, 121056. https://doi.org/10.1016/j.foreco.2023.121056.

Doughty, C.L., Cavanaugh, K.C., Chapman, S., Fatoyinbo, L., 2024. Uncovering mangrove range limits using very high resolution satellite imagery to detect fine-scale mangrove and saltmarsh habitats in dynamic coastal ecotones. Remote Sens. Ecol. Conserv. https://doi.org/10.1002/RSE2.394.

European Environmental Agency (EEA), 2014. Terrestrial habitat mapping in Europe: an overview. In: EEA Technical Report No 1/2014. https://doi.org/10.2800/11055.

Ferré, J., 2009. Regression diagnostics. Comprehens. Chemometr. 3, 33–89. https://doi.org/10.1016/B978-044452701-1.00076-4.

Ghosh, A., Fassnacht, F.E., Joshi, P.K., Kochb, B., 2014. A framework for mapping tree species combining hyperspectral and LiDAR data: role of selected classifiers and sensor across three spatial scales. Int. J. Appl. Earth Obs. Geoinf. 26 (1), 49–63. https://doi.org/10.1016/J.JAG.2013.05.017.

Giordano, E., Capitoni, B., Eberle, A., Maffei, L., Musicanti, A., Recanatesi, F., Torri, V., 2010. Forest management plan of the presidential Estate of Castelporziano. Segretariato Generale della Presidenza della Repubblica-Commissione Tecnico-Scientifica della Tenuta Presidenziale di Castelporziano 2010 (3), 131–398.

Girma, A., de Bie, C.A.J.M., Skidmore, A.K., Venus, V., Bongers, F., 2016. Hyper-temporal SPOT-NDVI dataset parameterization captures species distributions. Int. J. Geogr. Inf. Sci. 30 (1), 89–107. https://doi.org/10.1080/13658816.2015.1082565.

Gratani, L., Crescente, M.F., Varone, L., Puglielli, G., Catoni, R., Bonito, A., 2017. Carbon storage by Mediterranean vegetation developing inside a protected area. Rendiconti Lincei 28 (2), 425–433. https://doi.org/10.1007/S12210-017-0612-4/FIGURES/3.

Haboudane, D., Miller, J.R., Pattey, E., Zarco-Tejada, P.J., Strachan, I.B., 2004. Hyperspectral vegetation indices and novel algorithms for predicting green LAI of crop canopies: modeling and validation in the context of precision agriculture. Remote Sens. Environ. 90 (3), 337–352. https://doi.org/10.1016/J.RSE.2003.12.013.

Haddad, I., Soares Galvão, L., Marcelo Breunig, F., Dalagnol, R., Bourscheidt, V., Daniele Jacon, A., 2022. On the combined use of phenological metrics derived from different PlanetScope vegetation indices for classifying savannas in Brazil. https://doi.org/10.1016/j.rsase.2022.100764.

Hijmans, R.J., van Etten, J., Cheng, J., et al., 2015. Raster: Geographic Data Analysis and Modeling. http://CRAN.R-project.org/package=raster.

Hovi, A., Schraik, D., Kuusinen, N., Fabiánek, T., Hanuš, J., Homolová, L., Juola, J., Lukeš, P., Rautiainen, M., 2023. Synergistic use of multi- and hyperspectral remote sensing data and airborne LiDAR to retrieve forest floor reflectance. Remote Sens. Environ. 293, 113610. https://doi.org/10.1016/J.RSE.2023.113610.

Hua, J., Xiong, Z., Lowey, J., Suh, E., Dougherty, E.R., 2005. Optimal number of features as a function of sample size for various classification rules. Bioinformatics 21 (8), 1509–1515. https://doi.org/10.1093/BIOINFORMATICS/BTI171.

Huete, A., Didan, K., Miura, T., Rodriguez, E.P., Gao, X., Ferreira, L.G., 2002. Overview of the radiometric and biophysical performance of the MODIS vegetation indices. Remote Sens. Environ. 83 (1–2), 195–213. https://doi.org/10.1016/S0034-4257(02)00096-2.

Iglseder, A., Immitzer, M., Dostálová, A., Kasper, A., Pfeifer, N., Bauerhansl, C., Schöttl, S., Hollaus, M., 2023. The potential of combining satellite and airborne remote sensing data for habitat classification and monitoring in forest landscapes. Int. J. Appl. Earth Obs. Geoinf. 117. https://doi.org/10.1016/J.JAG.2022.103131.

Jarocińska, A., Kopeć, D., Niedzielko, J., Wylazłowska, J., Halladin-Dąbrowska, A., Charyton, J., Piernik, A., Kamiński, D., 2023. The utility of airborne hyperspectral and satellite multispectral images in identifying Natura 2000 non-forest habitats for conservation purposes. Sci. Rep. 13 (1). https://doi.org/10.1038/S41598-023-31705-6.

Karasiak, N., Dejoux, J.-F., Monteil, C., Sheeren, D., 2022. Spatial dependence between training and test sets: another pitfall of classification accuracy assessment in remote sensing, 111, 2715–2740. https://doi.org/10.1007/s10994-021-05972-1.

Kuhn, M., 2008. Building predictive models in R using the caret package. J. Stat. Softw. 28 (5), 1–26. https://doi.org/10.18637/JSS.V028.I05.

Kuhn, M., Johnson, K., 2013. Applied predictive modeling. Appl. Predict. Model. 448. https://doi.org/10.1007/978-1-4614-6849-3/COVER.

Kycko, M., Zagajewski, B., Kluczek, M., Tardà, A., Pineda, L., Palà, V., Corbera, J., 2022. Sentinel-2 and AISA airborne hyperspectral images for Mediterranean Shrubland mapping in Catalonia. Remote Sens. 14 (21), 5531. https://doi.org/10.3390/rs14215531.

Lang, N., Jetz, W., Schindler, K., Wegner, J.D., 2023. A high-resolution canopy height model of the Earth. Nat. Ecol. Evol. 7 (11), 1778–1789. https://doi.org/10.1038/s41559-023-02206-6.

Lazzeri, G., Frodella, W., Rossi, G., Moretti, S., 2021. Multitemporal mapping of post-fire land cover using multiplatform PRISMA hyperspectral and sentinel-UAV multispectral data: insights from case studies in Portugal and Italy. Sensors 21 (12), 3982. https://doi.org/10.3390/S21123982.

Le Dez, M., Robin, M., Launeau, P., 2021. Contribution of Sentinel-2 satellite images for habitat mapping of the Natura 2000 site 'Estuaire de la Loire' (France). Remote Sens. Appl. Soc. Environ. 24. https://doi.org/10.1016/J.RSASE.2021.100637.

Liaw, A., Wiener, M., 2002. Classification and Regression by randomForest, 2 (3). http://www.stat.berkeley.edu/.

Marcinkowska-Ochtyra, A., Ochtyra, A., Raczko, E., Kopeć, D., 2023. Natura 2000 grassland habitats mapping based on Spectro-temporal dimension of Sentinel-2 images with machine learning. Remote Sens. 15 (5). https://doi.org/10.3390/RS15051388.

Marian, M.L., Nasui, D., Ghise, C.R., Popovici, F., Sabo, C., Mare, R.O., Mihalescu, L., Vasilescu, B., Vosgan, Z., 2024. Using machine learning algorithms for natural habitats assessment. Carpathian J. Earth Environ. Sci. 19 (1), 103–113. https://doi.org/10.26471/CJEES/2024/019/282.

Marzialetti, F., Giulio, S., Malavasi, M., Sperandii, M.G., Acosta, A.T.R., Carranza, M.L., 2019. Capturing coastal dune natural vegetation types using a phenology-based mapping approach: the potential of Sentinel-2. Remote Sens. 11 (12). https://doi.org/10.3390/RS11121506.

Meerdink, S., Hiatt, D., Flory, S.L., Zare, A., 2024. Dealing with imperfect data for invasive species detection using multispectral imagery. Eco. Inform. 79, 102432. https://doi.org/10.1016/J.ECOINF.2023.102432.

Naimi, B., Hamm, N.A.S., Groen, T.A., Skidmore, A.K., Toxopeus, A.G., 2014. Where is positional uncertainty a problem for species distribution modelling? Ecography 37 (2), 191–203. https://doi.org/10.1111/J.1600-0587.2013.00205.X.

Peñuelas, J., Sardans, J., 2021. Global change and forest disturbances in the Mediterranean Basin: breakthroughs, knowledge gaps, and recommendations. Forests 12 (5), 603. https://doi.org/10.3390/F12050603.

Peñuelas, J., Filella, I., Biel, C., Serrano, L., Save, R., 1993. The reflectance at the 950-970 nm region as an indicator of plant water status. Int. J. Remote Sens. 14 (10), 1887–1905. https://doi.org/10.1080/01431169308954010.

Pepe, M., Pompilio, L., Gioli, B., Busetto, L., Boschetti, M., 2020. Detection and classification of non-photosynthetic vegetation from PRISMA hyperspectral data in croplands. Remote Sens. 12 (23), 3903. https://doi.org/10.3390/rs12233903.

Pesaresi, S., Mancini, A., Quattrini, G., Casavecchia, S., 2022. Functional analysis for habitat mapping in a special area of conservation using Sentinel-2 time-series data. Remote Sens. 14 (5). https://doi.org/10.3390/RS14051179.

Pesaresi, S., Mancini, A., Quattrini, G., Casavecchia, S., 2024. Evaluation and selection of multi-spectral indices to classify vegetation using multivariate functional principal component analysis. Remote Sens. 16 (7). https://doi.org/10.3390/RS16071224.

Pignatti, E., Ubrizsy Savoia, A., Pignatti, S., 2015. The landscape of Castelporziano at the time of the Roman empire: a testimony by Plinius the younger (second century AD). Rendiconti Lincei 26, 311–315. https://doi.org/10.1007/S12210-015-0390-9.

Prodromou, M., Theocharidis, C., Gitas, I.Z., Eliades, F., Themistocleous, K., Papasavvas, K., Dimitrakopoulos, C., Danezis, C., Hadjimitsis, D., 2024. Forest habitat mapping in Natura2000 regions in Cyprus Using Sentinel-1, Sentinel-2 and topographical features. Remote Sens. 16 (8). https://doi.org/10.3390/RS16081373.

Punalekar, S.M., Hurford, C., Lucas, R.M., Planque, C., Chognard, S., 2024. Hierarchical-modular framework for habitat mapping through systematic and informed integration of remote sensing data with contextual information. Eco. Inform. 82, 102714. https://doi.org/10.1016/J.ECOINF.2024.102714.

Quintano, C., Calvo, L., Fernández-Manso, A., Suárez-Seoane, S., Fernandes, P.M., Manuel Fernández-Guisuraga, J., 2023. First evaluation of fire severity retrieval from PRISMA hyperspectral data. Remote Sens. Environ. 295, 113670. https://doi.org/10.1016/j.rse.2023.113670.

Rapinel, S., Mony, C., Lecoq, L., Clément, B., Thomas, A., Hubert-Moy, L., 2019. Evaluation of Sentinel-2 time-series for mapping floodplain grassland plant communities. Remote Sens. Environ. 223, 115–129. https://doi.org/10.1016/J.RSE.2019.01.018.

Recanatesi, F., Giuliani, C., Rossi, C.M., Ripa, M.N., 2019. A remote sensing-assisted risk rating study to monitor pinewood forest decline: the study case of the castelporziano state nature reserve (Rome). Smart Innov. Syst. Technol. 100, 68–75. https://doi.org/10.1007/978-3-319-92099-3_9.

Recanatesi, F., Giuliani, C., Piccinno, M., Cucca, B., Rossi, C.M., Ripa, M.N., 2020. An innovative environmental risk assessment approach to a Mediterranean coastal

forest: the presidential Estate of Castelporziano (Rome) case study. Ann. Silvicult. Res. 44 (2), 80–85. https://doi.org/10.12899/asr-1884.
Rocchini, D., Balkenhol, N., Carter, G.A., Foody, G.M., Gillespie, T.W., He, K.S., Kark, S., Levin, N., Lucas, K., Luoto, M., Nagendra, H., Oldeland, J., Ricotta, C., Southworth, J., Neteler, M., 2010. Remotely sensed spectral heterogeneity as a proxy of species diversity: recent advances and open challenges. Eco. Inform. 5 (5), 318–329. https://doi.org/10.1016/J.ECOINF.2010.06.001.
Rocchini, D., Salvatori, N., Beierkuhnlein, C., Chiarucci, A., de Boissieu, F., Förster, M., Garzon-Lopez, C.X., Gillespie, T.W., Hauffe, H.C., He, K.S., Kleinschmit, B., Lenoir, J., Malavasi, M., Moudrý, V., Nagendra, H., Payne, D., Šímová, P., Torresani, M., Wegmann, M., Féret, J.B., 2021. From local spectral species to global spectral communities: a benchmark for ecosystem diversity estimate by remote sensing. Eco. Inform. 61, 101195. https://doi.org/10.1016/J.ECOINF.2020.101195.
Schweiger, A.K., Laliberté, E., 2022. Plant beta-diversity across biomes captured by imaging spectroscopy. Nat. Commun. 13 (1), 1–7. https://doi.org/10.1038/s41467-022-30369-6.
Scrinzi, G., Presutti Saba, E., Colle, G., 2016. Indirizzi Gestionali E Obiettivi D'intervento Per Le Classi Colturali Della Foresta Della Tenuta Presidenziale Di Castelporziano. Accademia Nazionale delle Scienze, Roma, Italy.
Scrinzi, G., Colle, G., Saba, E.P., Clementel, F., Maffei, L., Tinelli, A., Giordano, E., 2019. L'approccio lidar/GIS per la realizzazione dell'inventario forestale e del piano selvicolturale della foresta presidenziale di Castelporziano. L'Italia Forestale e Montana 74 (6), 341–356.
Simon, R., 2007. Resampling strategies for model assessment and selection. Fundament. Data Min. Genom. Proteom. 173–186. https://doi.org/10.1007/978-0-387-47509-7_8, 9780387475097.
Somers, B., Asner, G.P., 2014. Tree species mapping in tropical forests using multi-temporal imaging spectroscopy: wavelength adaptive spectral mixture analysis. Int. J. Appl. Earth Obs. Geoinf. 31, 57–66. https://doi.org/10.1016/j.jag.2014.02.006.
Strasser, T., Lang, S., 2015. Object-based class modelling for multi-scale riparian forest habitat mapping. Int. J. Appl. Earth Obs. Geoinf. 37, 29–37. https://doi.org/10.1016/J.JAG.2014.10.002.
Szostak, M., Likus-Cieślik, J., Pietrzykowski, M., 2021. PlanetScope imageries and LiDAR point clouds processing for automation land cover mapping and vegetation assessment of a reclaimed sulfur mine. Remote Sens. 13 (14), 2717. https://doi.org/10.3390/RS13142717.
Torresani, M., Rocchini, D., Sonnenschein, R., Zebisch, M., Marcantonio, M., Ricotta, C., Tonon, G., 2019. Estimating tree species diversity from space in an alpine conifer forest: the Rao's Q diversity index meets the spectral variation hypothesis. Eco. Inform. 52, 26–34. https://doi.org/10.1016/J.ECOINF.2019.04.001.
Tran, T.V., Reef, R., Zhu, X., Gunn, A., 2024. Characterising the distribution of mangroves along the southern coast of Vietnam using multi-spectral indices and a deep learning model. Sci. Total Environ. 923. https://doi.org/10.1016/J.SCITOTENV.2024.171367.
Tripathi, P., Garg, R.D., 2021. Feature extraction of desis and prisma hyperspectral remote sensing datasets for geological applications. In: International Archives of the Photogrammetry, Remote Sensing and Spatial Information Sciences - ISPRS Archives, 44(M–3), pp. 169–173. https://doi.org/10.5194/ISPRS-ARCHIVES-XLIV-M-3-2021-169-2021.
Vaglio Laurin, G., Zabeo, C., Giuliarelli, D., Tesfamariam, B.G., Cotrina-Sanchez, A., Valentini, R., Tufail, B., Ventura, B., Barbati, A., 2024. Monitoring Habitat Diversity with PRISMA Hyperspectral and Lidar-derived data in Natura 2000 Mediterranean Sites [Manuscript submitted for publication, Ecological Indicators].
Vangi, E., D'amico, G., Francini, S., Giannetti, F., Lasserre, B., Marchetti, M., Chirici, G., 2021. The new hyperspectral satellite PRISMA: imagery for forest types discrimination. Sensors 21 (4), 1182. https://doi.org/10.3390/S21041182.
Vanguri, R., Laneve, G., Hościło, A., 2024. Mapping forest tree species and its biodiversity using EnMAP hyperspectral data along with Sentinel-2 temporal data: an approach of tree species classification and diversity indices. Ecol. Indic. 167. https://doi.org/10.1016/J.ECOLIND.2024.112671.
Venier, L.A., Swystun, T., Mazerolle, M.J., Kreutzweiser, D.P., Wainio-Keizer, K.L., McIlwrick, K.A., Woods, M.E., Wang, X., 2019. Modelling vegetation understory cover using LiDAR metrics. PLoS One 14 (11), e0220096. https://doi.org/10.1371/JOURNAL.PONE.0220096.
Warren, S.D., Alt, M., Olson, K.D., Irl, S.D.H., Steinbauer, M.J., Jentsch, A., 2014. The relationship between the spectral diversity of satellite imagery, habitat heterogeneity, and plant species richness. Eco. Inform. 24, 160–168. https://doi.org/10.1016/J.ECOINF.2014.08.006.
Xia, F., Lv, G., 2024. Journal Pre-Proof Evaluation of Machine Learning Algorithm Capability for Bosten Lake Wetland Classification Based on Multi-Temporal Sentinel-2 Data. https://doi.org/10.1016/j.ecoinf.2024.102839.